ミュオン原子を用いた、
二重β崩壊核^{48}Caと^{48}Tiの電荷密度分布の測定

藤岡　宏之　（東京科学大学）

Institute of
SCIENCE TOKYO

Calcium-48

- One of five “stable” double magic nuclei (^{4}He, ^{16}O, ^{40}Ca, ^{48}Ca, ^{208}Pb)

  In this presentation, ^{48}Ca is regarded as stable because of its very long half-life.
- Calcium has many stable isotopes ranging from ^{40}Ca to ^{48}Ca.

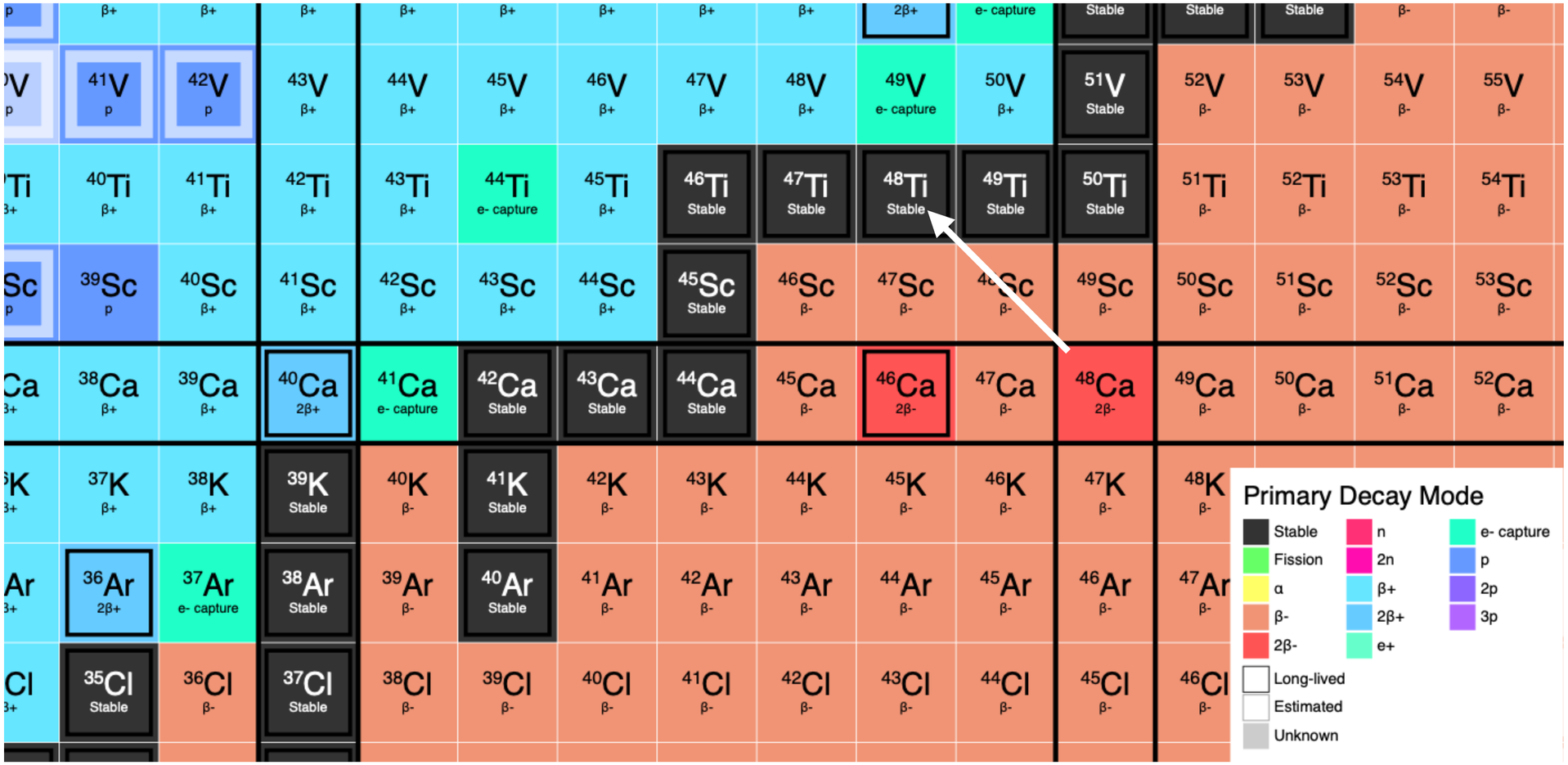

Proton/neutron density distributions of ^{40}Ca and ^{48}Ca

ab initio calculation

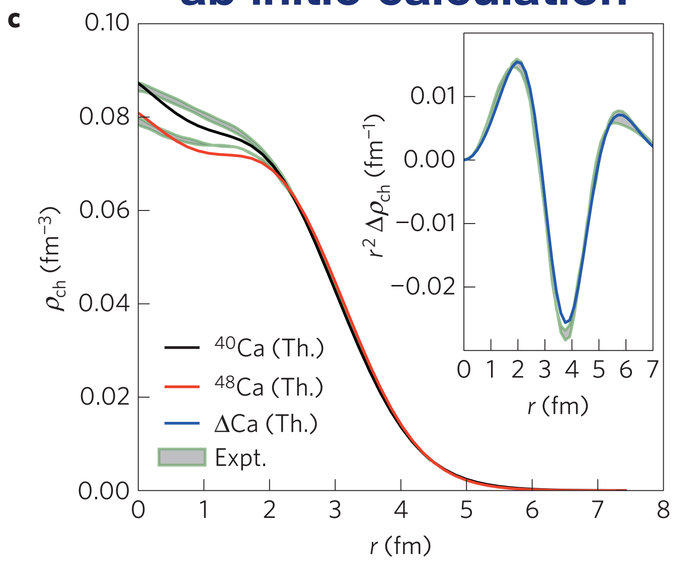

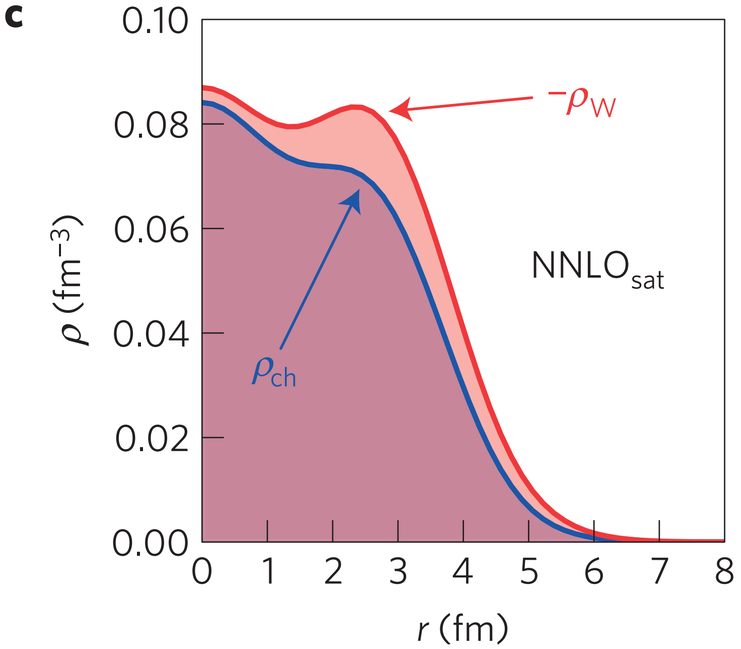

G. Hagen et al., Nature Physics 12 (2016) 186

proton scattering

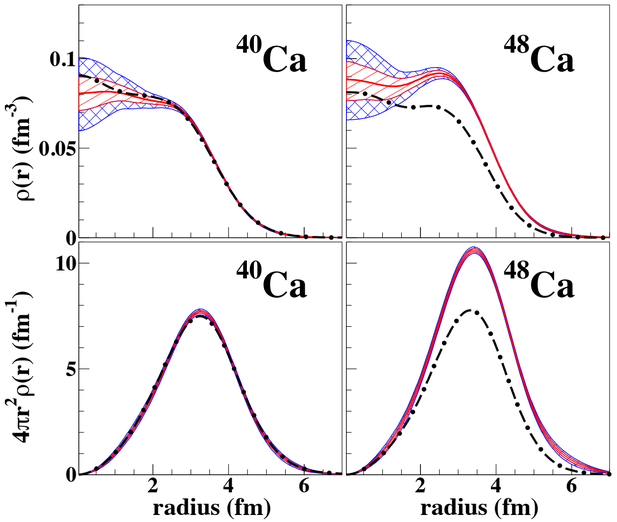

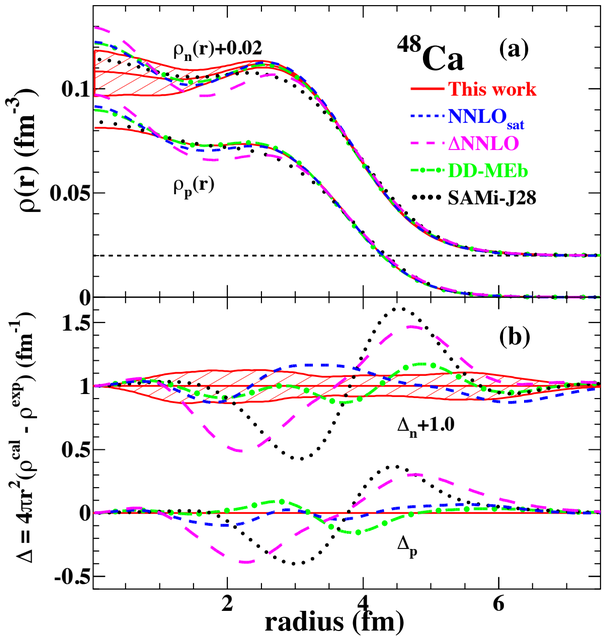

J. Zenihiro et al., arXiv:1810.11796

Nuclear charge radius

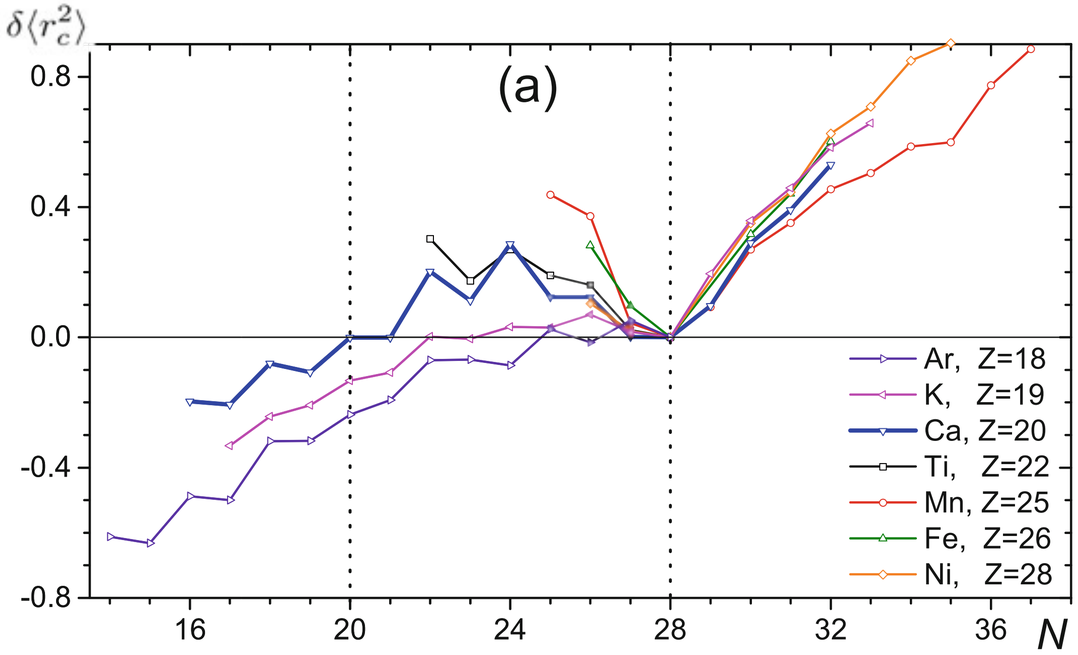

W. Nörtershäuser and I. D. Moore,
"Nuclear Charge Radii",
in "Handbook of Nuclear Physics"

- Usually, for isotopes with the same atomic number (Z),

  the rms charge radius $R_{\mathrm{ch}} = \sqrt{\langle r_{\mathrm{ch}}^2 \rangle}$ is a monotonically increasing function of N.

- However, this is not case for Ca isotopes. $R_{\mathrm{ch}}(^{40}\mathrm{Ca}) \approx R_{\mathrm{ch}}(^{48}\mathrm{Ca})$

Calculation with Skyrme models

Institute of SCIENCE TOKYO

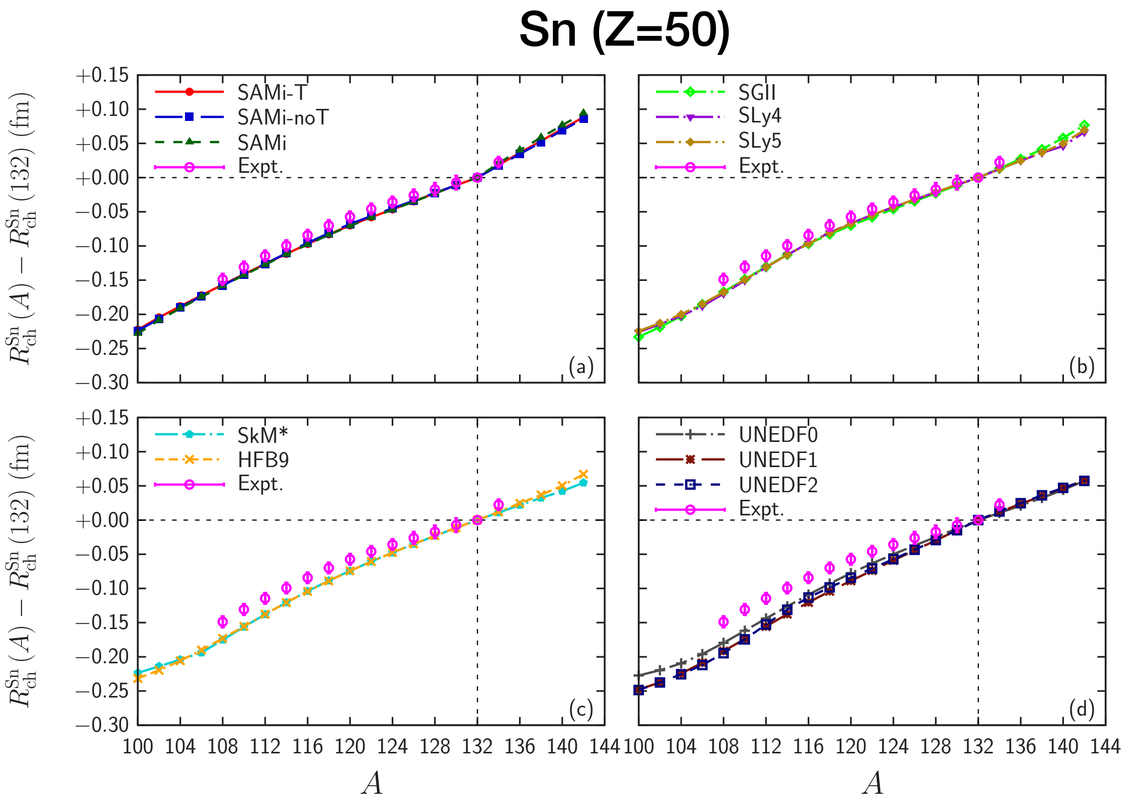

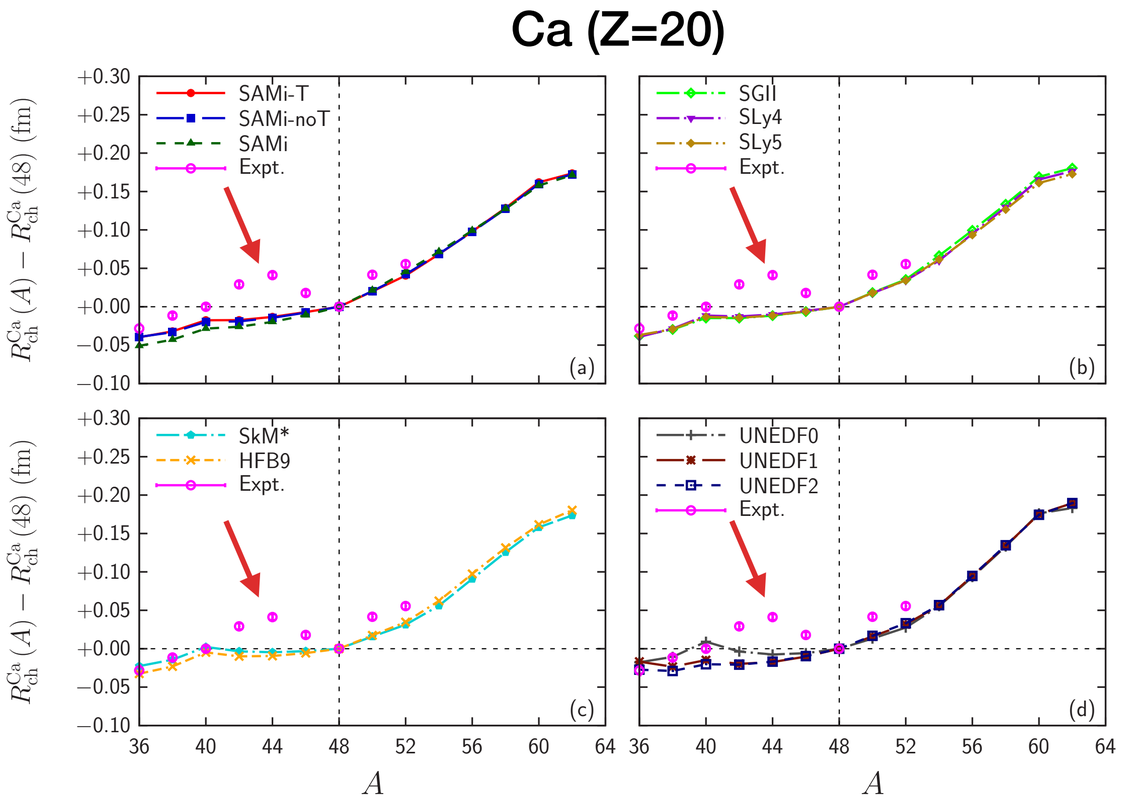

T. Naito et al., Phys. Rev. C **107**, 054307 (2023)

- $R_{\rm ch}(^{40}{\rm Ca}) \approx R_{\rm ch}(^{48}{\rm Ca})$ is reproduced in some models.
- The “arc behavior” between A=40 and 48 cannot be explained.

Experimental determination of charge radius

- Elastic electron scattering
  - $\rho_{\mathrm{ch}}(r)$ is determined from the form factor $F(q)$
- Muonic atom
  - Transition energies are largely affected by the finite size of the nucleus.
- Optical isotope shift
  - Transition frequencies is sensitive to $\langle r_{\mathrm{ch}}^2 \rangle$. The isotopic change of charge radii $\delta\langle r_{\mathrm{ch}}^2 \rangle^{A,A'} = \langle r_{\mathrm{ch}}^2 \rangle^{A'} - \langle r_{\mathrm{ch}}^2 \rangle^{A}$ can be evaluated.

G. Fricke and K. Heilig, “Nuclear Charge Radii”
W. Nörtershäuser and I. D. Moore,
“Nuclear Charge Radii” in “Handbook of Nuclear Physics”

Muon wave functions in muonic atoms

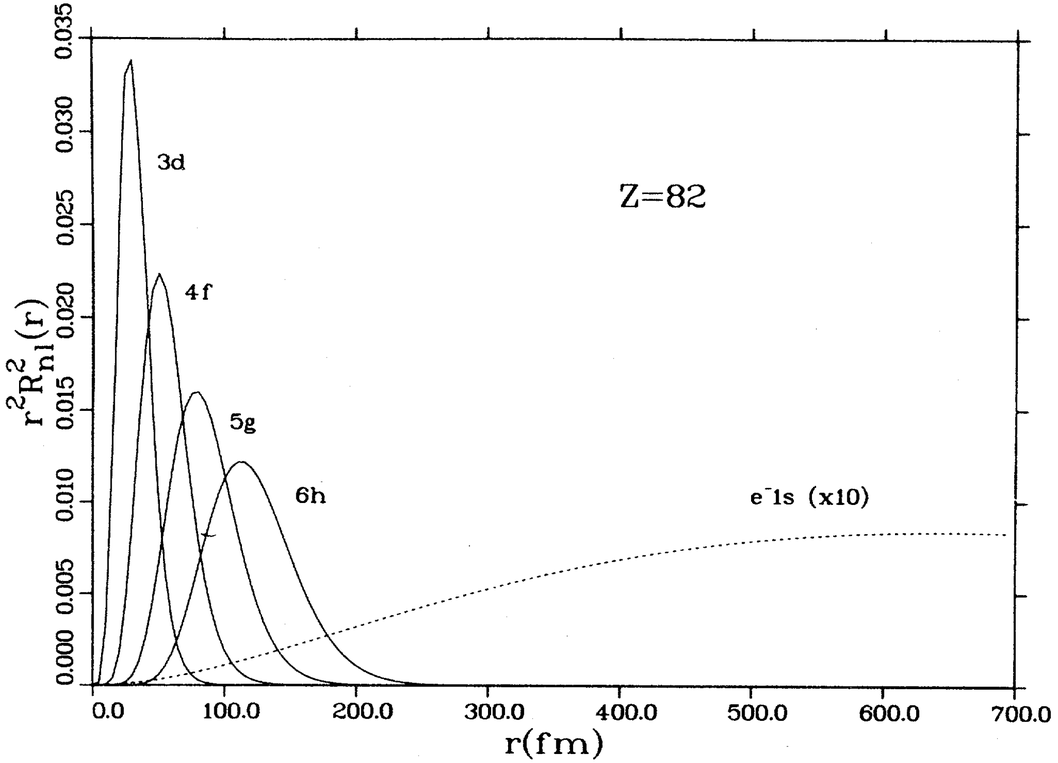

FIG. 1. Muon wave functions (solid lines) for relatively high-lying states, compared to the electron 1*s* wave function (dashed line).

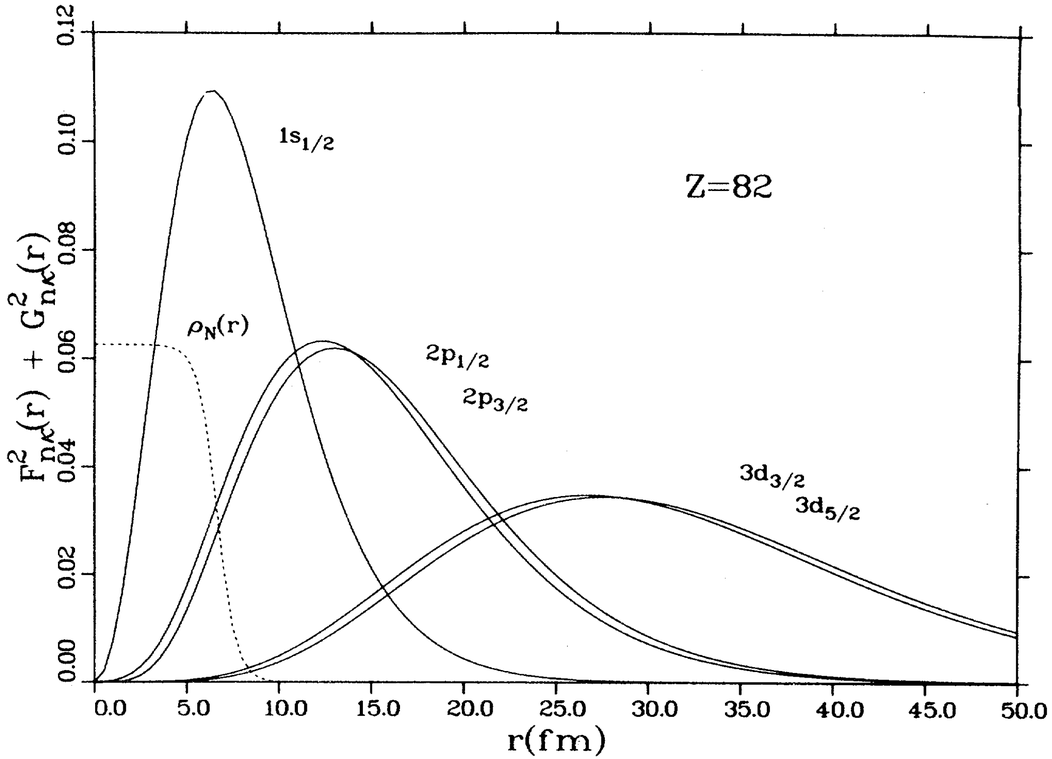

FIG. 2. Muon wave functions (solid lines) for relatively low-lying states, compared to the nuclear charge distribution $\rho_N(r)$ (dashed line).

E. Borie and G. A. Rinker, Rev. Mod. Phys. 54, 67 (1982)

Finite nuclear size effect on energy levels

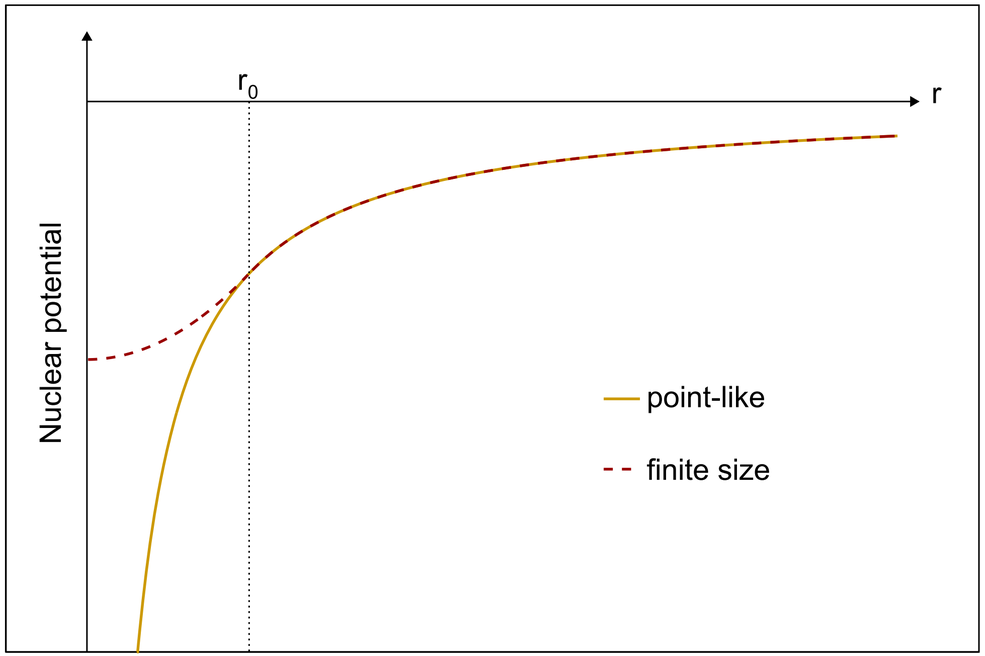

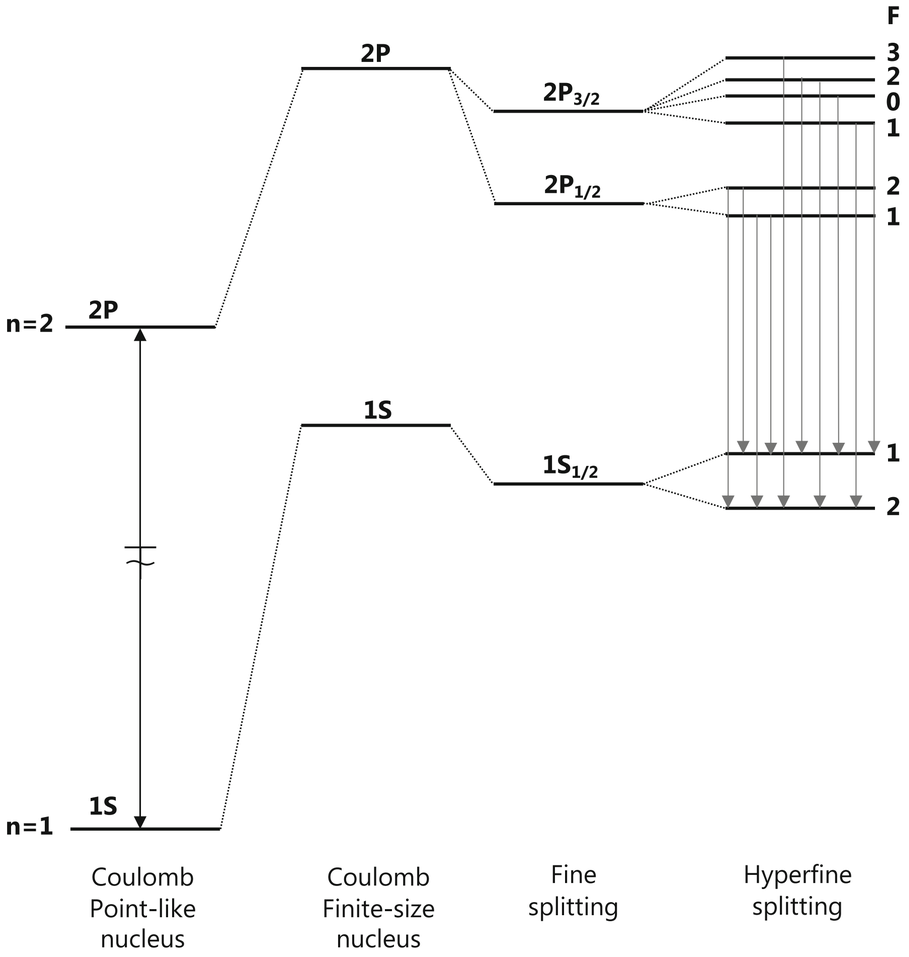

A. Knecht et al., Eur. Phys. J. Plus 135 (2020) 777

Related experiments

Institute of SCIENCE TOKYO

physics

MDPI

Communication

Towards Precision Muonic X-ray Measurements of Charge Radii of Light Nuclei

Ben Ohayon [1,*], Andreas Abeln [2], Silvia Bara [3], Thomas Elias Cocolios [3], Ofir Eizenberg [1], Andreas Fleischmann [2], Loredana Gastaldo [2], César Godinho [4,5], Michael Heines [3], Daniel Hengstler [2], Guillaume Hupin [5], Paul Indelicato [6], Klaus Kirch [7,8], Andreas Knecht [8], Daniel Kreuzberger [2], Jorge Machado [4], Petr Navratil [9], Nancy Paul [6,*], Randolf Pohl [10,11], Daniel Unger [2], Stergiani Marina Vogiatzi [8], Katharina von Schoeler [7,8] and Frederik Wauters [10,12]

1 Physics Department, Technion—Israel Institute of Technology, Haifa 3200003, Israel
2 Kirchhoff Institut für Physik, Universität Heidelberg, Im Neuenheimer Feld 227, 69120 Heidelberg, Germany
3 Katholieke Universiteit (KU) Leuven, Instituut voor Kern- en Stralingsfysica, 3001 Leuven, Belgium
4 Departamento de Física da Faculdade de Ciências e Tecnologia, Universidade Nova de Lisboa, Monte da Caparica, 2892-516 Caparica, Portugal
5 Le Laboratoire de Physique des Deux Infinis Irène Joliot-Curie (IJCLab), Centre National de la Recherche Scientifique/Institut National de Physique Nucléaire et de Physique des Particules (CNRS/IN2P3), Université Paris-Saclay, 91405 Orsay, France
6 Laboratoire Kastler Brossel, Sorbonne Université, CNRS, L'École-Normale Supérieure, Paris Sciences et Lettres (ENS-PSL) Research University, Collège de France, Case 74, 4, Place Jussieu, 75005 Paris, France
7 Institute for Particle Physics and Astrophysics, Eidgenössische Technische Hochschule (ETH) Zürich, 8093 Zürich, Switzerland
8 Paul Scherrer Institute, 5232 Villigen, Switzerland
9 TRIUMF, 4004 Wesbrook Mall, Vancouver, BC V6T 2A3, Canada
10 PRISMA+ Cluster of Excellence, Johannes Gutenberg-Universität Mainz, 55128 Mainz, Germany
11 Institut für Physik, QUANTUM, Johannes Gutenberg-Universität Mainz, 55128 Mainz, Germany
12 Institut für Kernphysik, Johannes Gutenberg-Universität Mainz, 55128 Mainz, Germany
* Correspondence: bohayon@technion.ac.il (B.O.); npaul@lkb.upmc.fr (N.P.)

QUARLET Collaboration, Physics 6 (2024) 206

Modern approach to muonic x-ray spectroscopy demonstrated through the measurement of stable Cl radii

K.A. Beyer,[1] T.E. Cocolios,[2] C. Costache,[3] M. Deseyn,[2] P. Demol,[4,5] A. Doinaki,[6,7] O. Eizenberg,[8] M. Gorshteyn,[9,10] M. Heines,[2,*] A. Herzáň,[11] P. Indelicato,[12] K. Kirch,[6,7] A. Knecht,[6] R. Lica,[3] V. Matousek,[11] E.A. Maugeri,[13] B. Ohayon,[8] N.S. Oreshkina,[1] W.W.M.M. Phyo,[2] R. Pohl,[10,14] S. Rathi,[8] W. Ryssens,[4,5] A. Turturica,[3] K. von Schoeler,[7] I.A. Valuev,[1] S.M. Vogiatzi,[2] F. Wauters,[9,10] and A. Zendour[6,7]

[1] *Max-Planck-Institut für Kernphysik, Heidelberg, Germany*
[2] *KU Leuven, Instituut voor Kern- en Stralingsfysica, Leuven, Belgium*
[3] *Horia Hulubei National Institute for R&D in Physics and Nuclear Engineering, Bucharest, Romania*
[4] *Université Libre de Bruxelles, Institut d'Astronomie et d'Astrophysique, Brussels, Belgium*
[5] *Brussels Laboratory of the Universe-BLU-ULB, Brussels, Belgium*
[6] *PSI Center for Neutron and Muon Sciences, Villigen, Switzerland*
[7] *ETH Zürich, Institute for Particle Physics and Astrophysics, Zürich, Switzerland*
[8] *The Helen Diller Quantum Center, Department of Physics, Technion-Israel Institute of Technology, Haifa, Israel*
[9] *Institut für Kernphysik, Johannes Gutenberg-Universität Mainz, Mainz, Germany*
[10] *PRISMA$^+$ Cluster of Excellence, Johannes Gutenberg-Universität Mainz, Mainz, Germany*
[11] *Institute of Physics, Slovak Academy of Sciences, Bratislava, Slovakia*
[12] *Laboratoire Kastler Brossel, Sorbonne Université, CNRS, ENS-PSL Research University, Collège de France, Paris, France*
[13] *PSI Center for Nuclear Engineering and Sciences, Villigen, Switzerland*
[14] *Institut für Physik, QUANTUM, Johannes Gutenberg-Universität Mainz, Mainz, Germany*

(Dated: June 12, 2025)

TABLE XIV: Resulting RMS radii of ^{35}Cl and ^{37}Cl (in fm and fm^2). For the pure muonic RMS radii, the V_2 is taken from the basic charge distribution model introduced in Section IV E.

Radius	Pure muonic	Using BSkG4	Literature [49]	Mirror estimates [13]
R^{35}	3.3325(48)	3.3335(23)	3.388(17)	3.323(11)
R^{37}	3.3448(48)	3.3445(23)	3.384(17)	3.338(7)
$R^{37} - R^{35}$	0.0128(64)	0.01154(98)	−0.004(24)	0.015(11)
$\delta\langle r^2\rangle^{37,35}$	0.085(43)	0.0771(66)	−0.03(16)	0.103(70)

arXiv:2506.08804

Reevaluation of charge radii of Calcium

- Naito et al. demonstrated that not only $\langle r_{\rm ch}^2 \rangle$ but also $\langle r_{\rm ch}^4 \rangle$ and the Barrett radius $R_{k\alpha}$ can be evaluated, even if the real density distribution is not a two-parameter Fermi distribution.

$$\rho(r) = \frac{\rho_0}{1 + \exp[4 \ln 3 (r - c)/t]}$$

Transition	$\Delta E_i^{\rm RCHB}$	^{40}Ca, $\Delta E_i^{\rm 2pf} - \Delta E_i^{\rm RCHB}$			
(keV)	(^{40}Ca)	2pf(σ_1)	2pf(R_2,σ_1)	2pf(R_2,σ_2)	2pf(R_2,R_4)
$2p_{3/2}$-$1s_{1/2}$	778.229	−2.58	1.82(−1)	8.47(−2)	3.69(−3)
$2p_{1/2}$-$1s_{1/2}$	776.766	−2.58	1.82(−1)	8.47(−2)	3.68(−3)
$3d_{3/2}$-$2p_{1/2}$	157.439	−8.03(−3)	−1.06(−3)	−4.46(−4)	7.14(−5)
$3d_{5/2}$-$2p_{3/2}$	156.124	−5.43(−3)	−1.11(−3)	−4.74(−4)	5.95(−5)
$3d_{3/2}$-$2p_{3/2}$	155.976	−5.43(−3)	−1.11(−3)	−4.74(−4)	5.96(−5)
$5f_{7/2}$-$3d_{5/2}$	79.851	−1.96(−6)	−6.14(−7)	−3.05(−7)	−5.66(−8)
$5f_{5/2}$-$3d_{5/2}$	79.835	−1.95(−6)	−6.05(−7)	−2.96(−7)	−4.78(−8)
$4f_{7/2}$-$3d_{5/2}$	54.599	−1.96(−6)	−6.07(−7)	−2.99(−7)	−5.04(−8)
$4f_{5/2}$-$3d_{5/2}$	54.568	−1.95(−6)	−6.06(−7)	−2.98(−7)	−4.95(−8)
$4d_{5/2}$-$3p_{1/2}$	55.074	−2.81(−3)	−3.70(−4)	−1.55(−4)	2.53(−5)
$4d_{5/2}$-$3p_{3/2}$	54.705	−1.91(−3)	−3.90(−4)	−1.66(−4)	2.13(−5)
$4d_{3/2}$-$3p_{3/2}$	54.643	−1.91(−3)	−3.90(−4)	−1.66(−4)	2.13(−5)

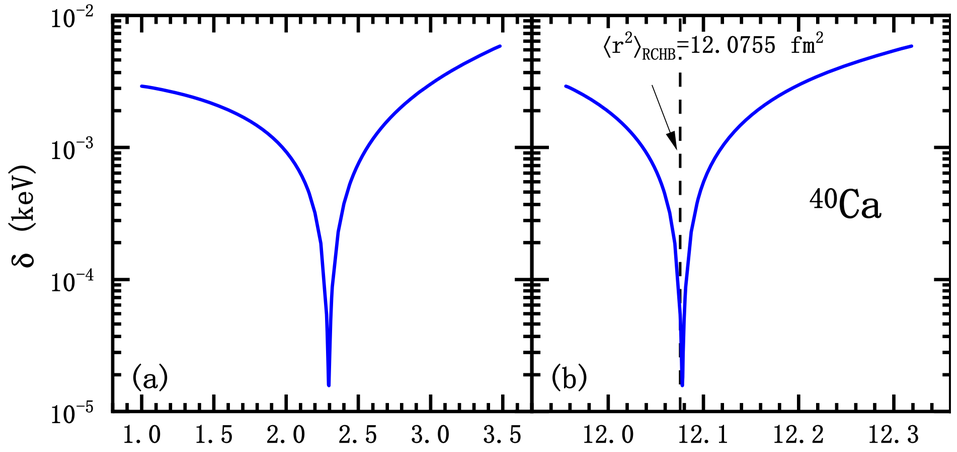

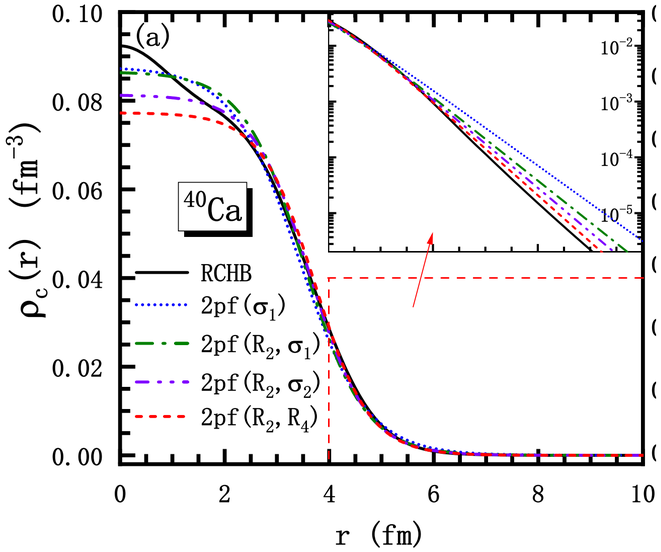

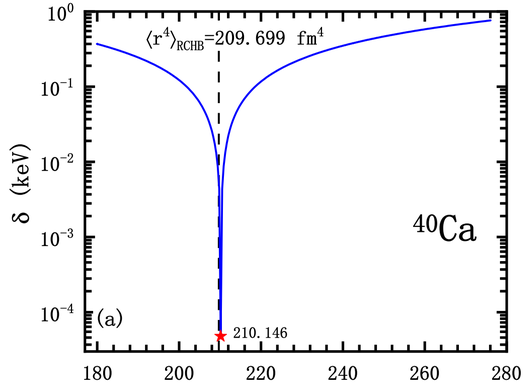

T. Naito et al., Phys. Lett. B 846 (2023) 138232

公募研究：X-ray spectroscopy of muonic Ca atoms

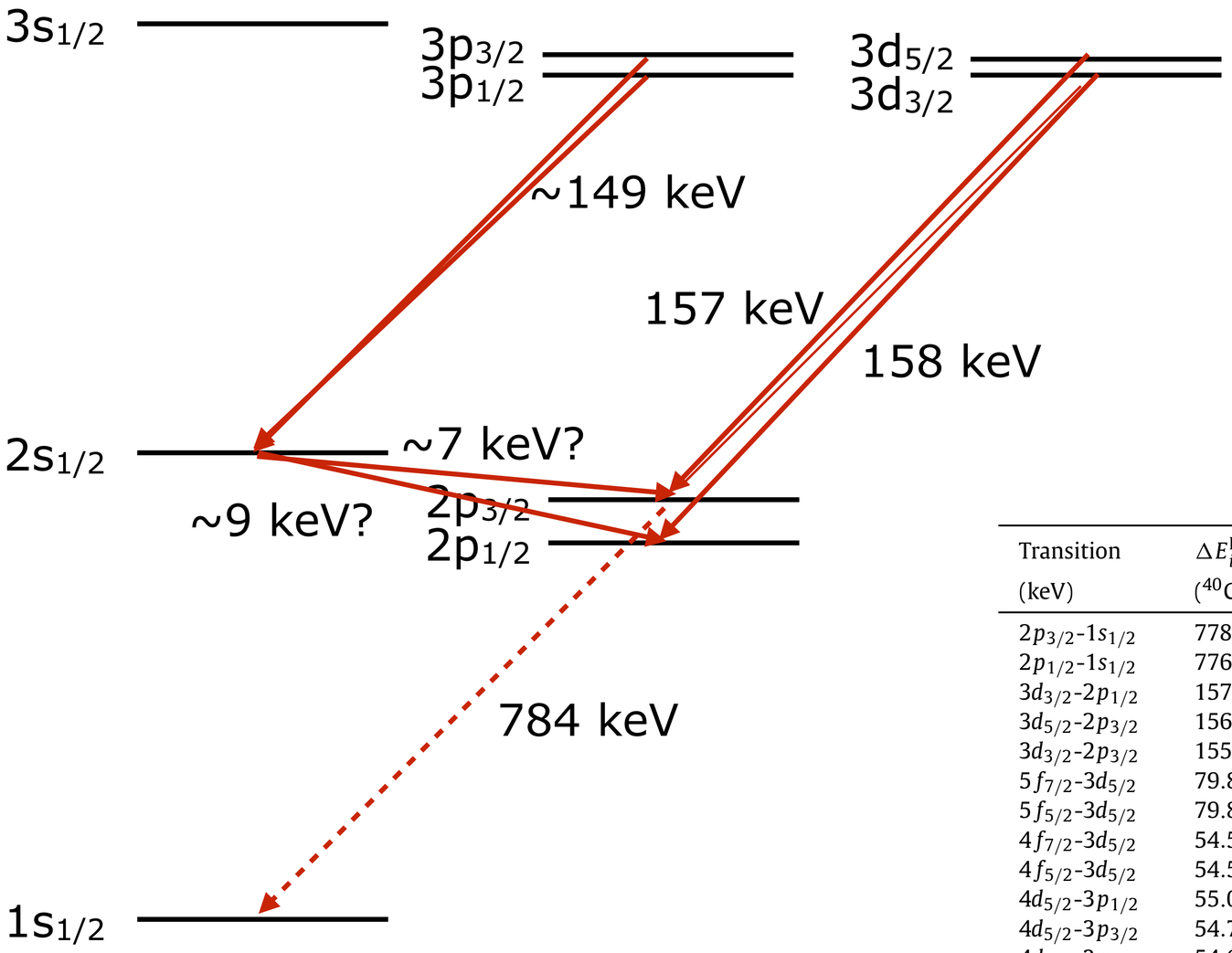

Transition (keV)	$\Delta E_i^{\mathrm{RCHB}}$ (^{40}Ca)	^{40}Ca, $\Delta E_i^{\mathrm{2pf}} - \Delta E_i^{\mathrm{RCHB}}$			
		2pf(σ_1)	2pf(R_2,σ_1)	2pf(R_2,σ_2)	2pf(R_2,R_4)
$2p_{3/2}$-$1s_{1/2}$	778.229	−2.58	1.82(−1)	8.47(−2)	3.69(−3)
$2p_{1/2}$-$1s_{1/2}$	776.766	−2.58	1.82(−1)	8.47(−2)	3.68(−3)
$3d_{3/2}$-$2p_{1/2}$	157.439	−8.03(−3)	−1.06(−3)	−4.46(−4)	7.14(−5)
$3d_{5/2}$-$2p_{3/2}$	156.124	−5.43(−3)	−1.11(−3)	−4.74(−4)	5.95(−5)
$3d_{3/2}$-$2p_{3/2}$	155.976	−5.43(−3)	−1.11(−3)	−4.74(−4)	5.96(−5)
$5f_{7/2}$-$3d_{5/2}$	79.851	−1.96(−6)	−6.14(−7)	−3.05(−7)	−5.66(−8)
$5f_{5/2}$-$3d_{5/2}$	79.835	−1.95(−6)	−6.05(−7)	−2.96(−7)	−4.78(−8)
$4f_{7/2}$-$3d_{5/2}$	54.599	−1.96(−6)	−6.07(−7)	−2.99(−7)	−5.04(−8)
$4f_{5/2}$-$3d_{5/2}$	54.568	−1.95(−6)	−6.06(−7)	−2.98(−7)	−4.95(−8)
$4d_{5/2}$-$3p_{1/2}$	55.074	−2.81(−3)	−3.70(−4)	−1.55(−4)	2.53(−5)
$4d_{5/2}$-$3p_{3/2}$	54.705	−1.91(−3)	−3.90(−4)	−1.66(−4)	2.13(−5)
$4d_{3/2}$-$3p_{3/2}$	54.643	−1.91(−3)	−3.90(−4)	−1.66(−4)	2.13(−5)

Previous measurement: 2p-1s transition

TABLE IV. Experimental equivalent radii R_k and Barrett moments $\langle r^k e^{-\alpha r}\rangle$ deduced from the $2p_{3/2}$-$1s_{1/2}$ transition energies. Fits were made using two-parameter Fermi charge distributions with a fixed at 0.55 fm. The theoretical nuclear polarization (NP) and quantum electrodynamic (QED) corrections used in the analysis are listed. The uncertainty in the nuclear polarization corrections, estimated to be 0.003 fm for the equivalent radii and 0.012 fm^k for the Barrett moments, are not included in the errors. The deduced rms radii are model dependent.

Isotope	Experimental transition energy (keV)	Correction NP (keV)	Correction QED (keV)	c (fm)	$\langle r^2\rangle^{1/2}$ (fm)	k	α (fm^{-1})	C_z (fm/keV)	R_k (fm)	C_z^* (fm^k/keV)	$\langle r^k e^{-\alpha r}\rangle$ (fm^k)
^{39}K	713.118(32)	0.145	5.324	3.5681	3.4378	2.114	0.064	−0.0499	4.4073(16)	−0.2276	10.666(7)
^{41}K	712.769(28)	0.150	5.305	3.5956	3.4549	2.114	0.064	−0.0499	4.4293(14)	−0.2276	10.767(6)
^{40}Ca	784.180(25)	0.170	5.907	3.6377	3.4813	2.114	0.065	−0.0420	4.4626(10)	−0.1922	10.879(5)
^{42}Ca	783.369(29)	0.196	5.891	3.6858	3.5115	2.114	0.065	−0.0420	4.5016(12)	−0.1922	11.057(6)
^{43}Ca	783.811(27)	0.181	5.897	3.6643	3.4980	2.114	0.065	−0.0420	4.4841(11)	−0.1922	10.977(5)
^{44}Ca	783.156(26)	0.205	5.886	3.7015	3.5214	2.114	0.065	−0.0420	4.5143(11)	−0.1922	11.116(5)
^{46}Ca	783.817(107)	0.208	5.897	3.6713	3.5024	2.114	0.065	−0.0420	4.4898(45)	−0.1922	11.003(21)
^{48}Ca	784.487(26)	0.190	5.905	3.6393	3.4823	2.114	0.065	−0.0420	4.4639(11)	−0.1922	10.884(5)
^{45}Sc	856.995(28)	0.233	6.489	3.7465	3.5498	2.116	0.066	−0.0356	4.5505(10)	−0.1649	11.270(5)
^{46}Ti	931.994(26)	0.285	7.093	3.8401	3.6094	2.118	0.068	−0.0307	4.6261(8)	−0.1419	11.563(4)
^{47}Ti	932.474(25)	0.265	7.099	3.8230	3.5984	2.118	0.068	−0.0307	4.6120(8)	−0.1419	11.498(4)
^{48}Ti	932.652(26)	0.284	7.103	3.8185	3.5956	2.118	0.068	−0.0307	4.6083(8)	−0.1419	11.481(4)
^{49}Ti	933.426(33)	0.237	7.113	3.7892	3.5770	2.118	0.068	−0.0307	4.5843(10)	−0.1419	11.370(5)
^{50}Ti	933.588(26)	0.253	7.114	3.7851	3.5743	2.118	0.068	−0.0307	4.5809(8)	−0.1419	11.354(4)
^{51}V	1012.201(26)	0.296	7.758	3.8307	3.6033	2.116	0.069	−0.0265	4.6173(7)	−0.1219	11.448(3)
^{50}Cr	1091.178(27)	0.392	8.391	3.9262	3.6645	2.115	0.071	−0.0232	4.6947(6)	−0.1063	11.698(3)
^{52}Cr	1092.286(21)	0.353	8.408	3.8962	3.6452	2.115	0.071	−0.0232	4.6698(5)	−0.1063	11.584(2)
^{53}Cr	1091.381(25)	0.342	8.391	3.9222	3.6620	2.115	0.071	−0.0232	4.6914(6)	−0.1063	11.683(3)
^{54}Cr	1089.888(31)	0.386	8.366	3.9661	3.6902	2.115	0.071	−0.0232	4.7278(7)	−0.1063	11.850(3)
^{55}Mn	1172.854(34)	0.396	9.041	3.9962	3.7096	2.120	0.072	−0.0203	4.7527(7)	−0.0945	11.999(3)
^{56}Fe	1257.042(25)	0.459	9.715	4.0449	3.7412	2.121	0.074	−0.0181	4.7921(5)	−0.0834	12.102(2)

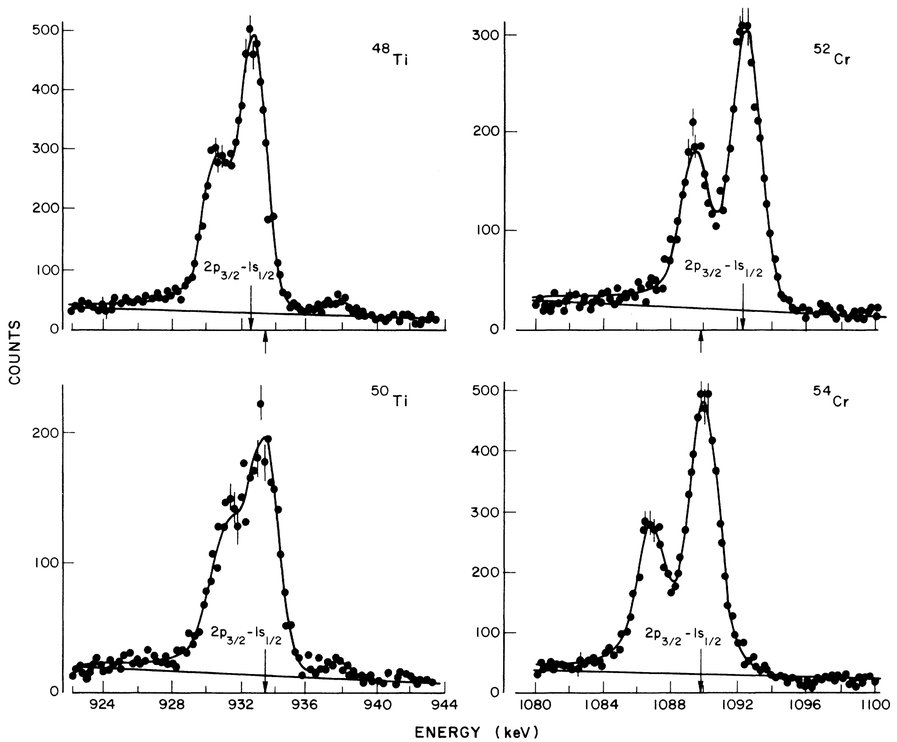

FIG. 2. Typical spectra showing the muonic $2p$-$1s$ x-ray doublet for Ti and Cr isotopes. The shifts of the x-ray energies are seen to have opposite signs for ^{50}Ti-^{48}Ti and ^{54}Cr-^{52}Cr. The substantial (24%) ^{48}Ti contamination of the ^{50}Ti target is visible. The curves show fits to the measured spectra. The weak line at about 937.5 keV is caused by feedthrough of the ^{110}Ag^m calibration source.

H.D. Wohlfahrt, E.B. Shera, M.V. Hoehn, Y. Yamazaki, R.M. Steffen, Phys. Rev. C 23 (1981) 533.

Previous measurement: 3d-2p transition

Institute of SCIENCE TOKYO

M.S. Dixit et al., Phys. Rev. Lett. 27 (1971) 878

Z	Element	Transition	Finite Size Effect	Vacuum Polarization of Order α	Vacuum Polarization Higher Order $(\alpha_1^2(Z\alpha)^3)$	$E_{total(theory)}$	$E_{experiment}$	$\Delta E_{theory-exp.}$ (eV) (discrepancy ppm)
20	Ca	$3d_{3/2} \rightarrow 2p_{1/2}$	-.078	0.734	.006	158.181±.003	158.173±.018	8 ± 18 (51±114)
		$3d_{5/2} \rightarrow 2p_{3/2}$	-.028	0.716	.006	156.845±.002	156.830±.016	15 ± 16 (96±102)
22	Ti	"	-.154	0.947	.009	191.921±.006	191.921±.018	0 ± 19 (0 ± 99)
			-.058	0.920	.009	189.977±.004	189.967±.017	10 ± 18 (53± 95)

Ge(Li) detector with resolution of 600 eV @ 136 keV

C.K. Hargrove et al., Phys. Rev. Lett. 39 (1977) 307

TABLE I. Comparison of the experimental and calculated transition energies for several muonic atoms which are sensitive to the vacuum-polarization correction. The theoretical numbers are from Ref. 6. The weighted deviation of all transitions, as a fraction of the vacuum-polarization correction, is 0.0018 ± 0.0015.

Transition		Experiment (eV)	Theory (eV)	Vacuum polarization (eV)	Theory − experiment (eV)
Ca	$3d$–$2p$	156 842.4± 5.2	156 845± 3	716	2.6± 6.0
		158 171.6± 6.6	158 182± 4	734	10.4± 7.7
Ba	$5g$–$4f$	199 917.3± 4.8	199 907± 3	748	−10.3± 5.7
		201 274.7± 7.1	201 274± 3	762	− 0.7± 7.7

Ge detector with resolution of 870 eV @ 316 keV

TES (Transition Edge Sensor) microcalorimeter

Institute of SCIENCE TOKYO

川崎 海斗, ポスター発表 P20

Re-evaluation of nuclear charge density distribution with precision measurement of X-rays using TES microcalorimeters

研究目標・計画

- ^{48}Ca (天然存在比 0.187%) は非常に高額
- 目標：CANDLES実験（計画研究A02) で開発中の^{48}Ca同位体濃縮技術で濃縮された^{48}Caを提供してもらい、また濃縮^{48}Tiを購入し、J-PARC MLF でミュオンビームを用いた実験を行う。
  - ▷ 濃縮した^{48}Caをどのようにして取り出して実験標的にするか検討
  - ▷ mudirac をベースに、ミュオニック原子のエネルギー準位を計算
    [GitHub] https://github.com/muon-spectroscopy-computational-project/mudirac
  - ▷ 計画研究E01との連携 (?) : ^{48}Ca, ^{48}Tiの電荷密度分布と0νββ崩壊の核行列要素との関連？
- 2025年度4-5月に, CaF_2 (^{40}Ca) を用いた短時間の測定（→川崎海斗 ポスター発表P20）
  - ▷ $3d_{3/2}$-$2p_{1/2}$, $3d_{5/2}$-$2p_{3/2}$ 遷移のピークを確認

結論

- カルシウム原子核の荷電半径の質量数依存性が他の元素とは大きく異なる
- ミュオン原子のX線分光を通じて、カルシウム同位体の電荷密度分布（荷電半径 $R_{\mathrm{ch}} = \sqrt{\langle r_{\mathrm{ch}}^2 \rangle}, \langle r_{\mathrm{ch}}^4 \rangle$, Barrett半径）の再評価を行いたい。
- 本研究では特に^{48}Caと^{48}Tiに焦点を当てて研究を進めていく。
- 0νββ崩壊の核行列要素$M^{0\nu}$との関連についても議論していきたい。

謝辞：本研究はMEXT科研費25H02178の助成を受けたものです。

Barrett radius

- The shift of the transition energy in muonic atoms due to a variation of the spherical nuclear charge distribution, $\delta\rho(r)$, is expressed as:

$$\Delta E_{\mathrm{if}} = 4\pi \int \delta\rho(r)[V^{\mathrm{i}}(r) - V^{\mathrm{f}}(r)]r^2 dr$$

- The potential difference $V^{\mathrm{i}}(r) - V^{\mathrm{f}}(r)$ can be approximated by $Br^k e^{-\alpha r}$.
- The Barrett moment $\langle r^k e^{-\alpha r} \rangle$ is insensitive to the detail of the nuclear charge distribution.
- An equivalent Barrett radius $R_{k\alpha}$, which satisfies the following relation, is used in literature.

$$\langle r^k e^{-\alpha r} \rangle = \frac{3}{R_{k\alpha}^3} \int_0^{R_{k\alpha}} r^k e^{-\alpha r} r^2 dr$$